ACS OMEGA

http://pubs.acs.org/journal/acsodf

Article

Nickel–Cobalt Oxide Nanoparticle-Induced Biohydrogen Production

Zhenmin Li, Jiangmei Wang, Kexin Tian, Chen Zhou, Yong Pei, Jishi Zhang,* and Lihua Zang

Cite This: *ACS Omega* 2022, 7, 41594–41605

Read Online

ACCESS | Metrics & More | Article Recommendations

ABSTRACT: The positive effects of metal oxide nanoparticles (NPs) on dark fermentation (DF) for biohydrogen synthesis have been increased, and the mechanism still needs to be further revealed. In this study, nickel–cobalt oxide ($NiCo_2O_4$) NPs were prepared to increase H_2 yield via DF. The highest (259.67 mL/g glucose) and the lowest (188.14 mL/g glucose) yields were achieved at 400 and 800 mg/L $NiCo_2O_4$ NPs added, respectively, with their corresponding 33.97% increase and 2.93% decrease compared with the control yield (193.82 mL/g glucose). Meanwhile, the microbial community further confirmed that $NiCo_2O_4$ NPs increased the abundance of the dominant H_2-producing *Clostridium sensu stricto1* by 23.05%. The gene prediction also showed that $NiCo_2O_4$ NPs increased the abundance of genes encoding the rate-limiting enzyme pyruvate kinase in glycolysis, thus increasing the substrate conversion. Moreover, the gene abundance of key enzymes directly related to H_2 evolution was also increased at different levels.

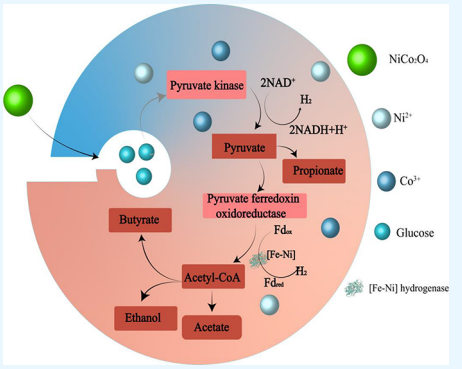

1. INTRODUCTION

As more and more machines gradually replace human labor, the increasing level of mechanization and industrialization inevitably leads to environmental pollution and other problems.[1] In particular, the CO_2 produced from the use of coal, oil, and natural gas has led to global warming, increased sea levels, and even the extinction of some species.[2] The emergence of extreme weather may occur, which threatens the normal life and production of human beings.[3] Moreover, the increasing requirement for energy from a growing world population increases the pressure on the environment and energy. The above serious situation has forced people to accelerate the development of new energy sources for the eco-friendly and sustainable development of humans. Considering the cleanliness and sustainability of H_2 consumption, H_2 yield and storage technology have received widespread attention.[4]

H_2 can be produced by electrolysis of water, photosynthetic H_2 evolution, industrial by-product reforming, and biofermentation.[5] The sophisticated types of equipment and high capital investment that are required for the previous three methods limited the possibility of industrial application. Researchers have been looking for a low-cost and easy-to-operate process to produce H_2.[6] Biofermentation for H_2 production includes dark fermentation (DF), photo-assisted process, and their combination. Although the latter two processes are faster in H_2 synthesis and have higher substrate conversion rates, both involve the use of light sources, likely causing light pollution to the environment.[7,8] In contrast, the DF is not only rapid and efficient in the substrate conversion to H_2 and volatile fatty acids (VFAs) but also employs kitchen residue, agricultural waste, and organic wastewater to obtain H_2.[9] This measure alleviates environmental pollution, recovers some energy, and reduces the exploitation of nonrenewable energy sources.

Nonetheless, the actual H_2 yield from DF was much lower than its theoretical value of 4 mol/mol glucose.[10] This is due to the fact that (a) glucose may not be metabolized by the biochemical process of H_2 evolution; (b) a part of glucose is consumed by the bacteria of assimilating microbes; and (c) the produced H_2 is likely employed by the H_2-consuming microbes. The high yield of H_2 from DF can be improved by boosting the activity of relevant microbes. For example, by adding microelements (e.g., Co, Ni, Fe, Mn, Zn) essential for germs to the DF reactor.[11] In addition, it has been revealed that metal NPs can not only interact with enzymes or membrane proteins on cells but also act as extracellular electron acceptors in cellular metabolic processes.[12] Previous reports revealed that NPs had the quantum size effect (QSE) and high surface area (HSA), and conductive NPs could quicken the electron transfer (ET) between cells, within microbes and between enzymes at lower concentration levels.[13,14]

Based on the aforementioned factors, many researches were conducted to explore the influence of monometallic trace element-induced NPs on H_2 evolution in DF reactors and found that the H_2 generation was significantly enhanced. For

Received: August 29, 2022
Accepted: October 21, 2022
Published: November 1, 2022

example, some NPs released Ni^{2+}, Fe^{0}, and Fe^{2+} and increased H_2 yields by 55, 37, and 15%, respectively, in contrast with the control yield.[15] Cobalt (Co) is the vital element of coenzyme B_{12} ($C_{72}H_{100}CoN_{18}O_{17}P$), and its adequate dosage can evidently alleviate the accumulation of VFAs in DF, indicating that the appropriate Co-induced DF reaction favors microbial activity.[16] Zhang et al.[17] discovered that NiO NPs extracted from *Eichhornia crassipes* increased the H_2 production rate (HPR) by 47.29% compared with the control yield of mesophilic DF.[17] In addition, ferredoxin hydrogenase was extremely crucial in the DF for producing H_2, and Yang et al.[18] revealed that an appropriate dosage of lanthanum−iron oxide NPs was favorable for the synthesis of ferredoxin hydrogenase via DF.[18] Hydrogenase is the key enzyme in catalytic DF that converts the NADH produced along with the decomposition of glucose into H_2 and NAD^+.[19] They are mainly divided into [Ni−Fe] and [Fe−Fe] hydrogenase in view of the central active metal, and the former was more frequently found in microbes than the latter.[15,20] It has been reported that the addition of alkali-based magnetic nanosheets to the DF reactor at mesophilic and thermophilic conditions increased the activities of hydrogenase by 10.5 and 42.8% and their H_2 yields by 65.4 and 43.3%, respectively.[21] The reason for the promoting effect of nickel on bioH_2 production was described as the metal cofactor of the active center of [Ni−Fe] hydrogenase.[22] Also, the work illustrated that the addition of Ni NPs and Ni−graphene nanocomposite to industrial wastewater could increase H_2 yield by 23 and 105%, respectively.[22] Nanoscale metal oxides are less toxic to microbess than pure metal NPs.[23] The related study on the DF for H_2 generation amended with TiO_2 was performed by Hsieh et al.,[24] where the stimulation mechanism attributed to the ET within the H_2−DF of *Clostridium pasteurianum*.[24]

Nevertheless, to our knowledge, $NiCo_2O_4$ NPs not have been reported for bioH_2 production by the DF reaction. Therefore, the main tasks in this work are (a) to synthesize $NiCo_2O_4$ NPs and characterize them; (b) to reveal the influence on bioH_2 production by DF under 37 °C conditions in different dosages of $NiCo_2O_4$ NPs; (c) to detect and analyze the intermediate products in the DF process; (d) to uncover the microbial community variation at different doses of $NiCo_2O_4$ NPs; and (e) to predict the functional genes for bacteria after the DF procedure.

2. MATERIALS AND METHODS

2.1. Inoculums Production. The inoculums used for this work were obtained from the wastewater-containing citric acid treatment plant in Shandong of China. To breed H_2-producing bacteria (HPB), the inoculated sludge needs to be domesticated and cultured in anaerobic condition at 37 °C without nutrients for 20 days and then an oil bath for 45 min at 90 °C for enriching HPB and restraining methanogens. Then, the preheated sludge was cooled to 37 °C, and 1.0 g/L of glucose was added followed by DF at 37 °C for 48 h. Thus, the inoculums of H_2−DF were obtained and then characterized for its physicochemical properties based on the methods of Sun et al.[25] and the results are presented in Table 1.

2.2. $NiCo_2O_4$ NPs Preparation. The $NiCo_2O_4$ NPs used in this work were fabricated by sol−gel means. The specific process was as follows: (a) $Ni(NO_3)_2{\cdot}6\ H_2O$ (0.01 mol, 2.91 g) and Co $(NO_3)_2{\cdot}6\ H_2O$ (0.02 mol, 5.83 g) were fully dissolved in 60 mL of deionized water. (b) Citric acid monohydrate (0.045 mol, 9.46 g) was mixed with the above solution and stirred to form a stable and clear liquid. (c) Ammonia was added slowly dropwise to regulate the pH to 2.0, and the liquid was stirred at 80 °C for 120 min to produce a gel and then dried in a drying cabinet at 115 °C for 300 min. (d) The intermediate was incinerated at 700 °C for 4.5 h; subsequently, the calcined sample was cooled to room temperature and purified with deionized water and ethanol alternately 2 times. (e) The purified product was dried under vacuum conditions at 60 °C, and then $NiCo_2O_4$ NPs were obtained, which were milled into powder and stored in an airtight condition.

Table 1. Physicochemical Properties of Inoculated Sludge

physical and chemical indexes	seed sludge
pH	7.0 ± 0.1
total solid (TS, wt.%)	12.5 ± 0.3
volatile solid (VS, wt.% of TS)	52 ± 0.8
chemical oxygen demand (COD, mg/L)	7289 ± 55
total organic carbon (TOC, mg/L)	2569 ± 60
total carbon (TC, mg/L)	3074 ± 70
inoraganic carbon (IC, mg/L)	505 ± 25
ammonium (NH_4^+−N, mg/L)	476 ± 15

2.3. Batch Fermentation Process. Three sets of parallel experiments were designed for this study. All DF tests were conducted in the 500 mL DF reactor with a remaining volume of 125 mL for reducing the DF H_2 partial pressure. Then, inoculum (150 mL) and substrate (glucose 10 g/L, peptone 0.3 g/L) were added to each DF reactor. In addition, seven concentration gradients of $NiCo_2O_4$ NPs (0, 50, 100, 200, 400, 600, and 800 mg/L) were added to the above reactor to evaluate the effect on bioH_2 yield from DF at 37 °C. The initial pH values of all reactors were near neutral (7.0) without regulation. To provide an anaerobic environment for microbes, all reactors were purged with nitrogen for 3 min and sealed quickly, and then they began to produce H_2 under mesophilic conditions (37 °C) and lasted for 36 h. Finally, the generated H_2 was collected by the saturated NaOH solution to remove the interference of acidic gases such as CO_2 and H_2S. The H_2 yields were determined every 3 h, while fermentation liquids were sampled every 6 h for chemical characterization. Moreover, H_2 measurement and determination need to follow a previous work.[26]

2.4. Determination of $NiCo_2O_4$ NP Characteristics. The crystal structure and phase component of $NiCo_2O_4$ NPs were revealed with an X-ray diffraction (XRD, AXS, Bruker, Germany) at an angle of 2θ in the range of 10−80°, maintaining a scanning rate of 20°/min. $NiCo_2O_4$ NPs were analyzed by the versatile scanning electron microscopy (SEM) (S4800, Hitachi, Japan) with an energy dispersive spectrometer (EDS) (X-MAX80, Oxford, UK) for their morphological and elemental composition, where the EDS model was Xplore, and the gold spray target was a platinum target. The surface area of $NiCo_2O_4$ NPs was estimated by the Brunauer−Emmett−Teller detector (BET, ASAP2460, Micromeritics, USA). In addition, the elemental composition and chemical states of $NiCo_2O_4$ NPs were revealed through an X-ray photoelectron spectrometer (XPS, ESCALAB 250Xi, Thermo Scientific, USA) using Al Kα X-rays as the excitation source.

2.5. Liquid Analysis. The key physicochemical indicators of seed sludge, such as total organic carbon (TOC), inorganic carbon (IC), total solids (TS), volatile solids (VS), ammonium (NH_4^+−N), pH, and chemical oxygen demand (COD) were

https://doi.org/10.1021/acsomega.2c05580
ACS Omega 2022, 7, 41594−41605

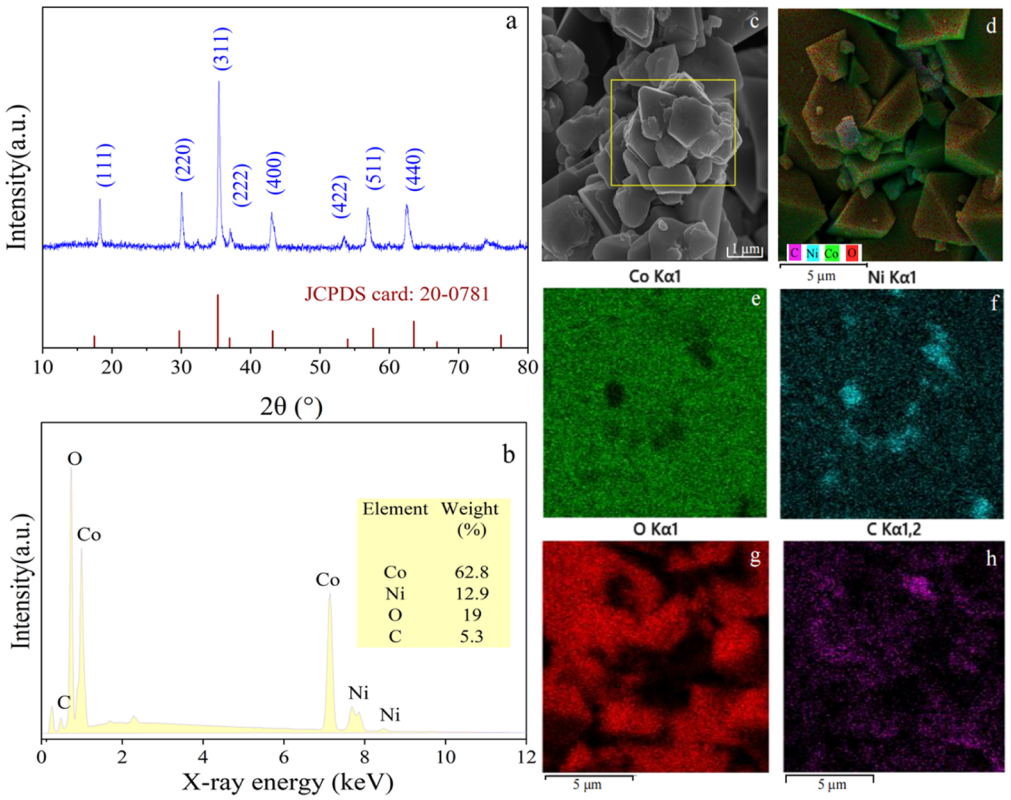

Figure 1. $NiCo_2O_4$ NPs XRD graphic (a); SEM−EDS graphic of $NiCo_2O_4$ NPs (b); SEM graphic of $NiCo_2O_4$ NPs at 1 μm (c); element distribution of SEM mapping (d−h).

gauged consistent with the former methods.[21] First of all, the collected samples of fermentation broth were centrifuged at 7000 r/min for 5 min and then filtrated with a filter membrane with a pore size of 0.45 μm. The SMPs such as HAc (acetate), HPr (propionate), HBu (butyrate), EtOH (ethanol), and glucose were evaluated by high-performance liquid chromatography (HPLC, LC-20AT, Shimadzu, Japan) with a detector of refractive index. Sulfuric acid (0.005 M, 0.5 mL/min) was utilized as the mobile phase, which was equipped with an Aminex HPX-87H column and Cation-H cartridge micro-guard. The contents of nickel and cobalt ions in the zymotic fluid were determined by an inductively coupled plasma emission spectrometer (ICP−OES, Optima 7000DV, Perkin Elmer, MA, USA).

2.6. Three-Dimensional Fluorescence Assay and 16S rRNA Gene Amplicon Sequencing. The extracellular polymers (EPS) were extracted from the final sludge after DF and based on previous techniques,[27] which were obtained from the control, the highest, and the lowest H_2 yield samples. To determine the EPS characteristics, these sludge samples (15 mL) were centrifuged (6000 r/min, 10 min), and they were dissolved in Ringer solution (150 mmol/L NaCl, 2.5 mmol/L $CaCl_2$, 4.0 mmol/L KCl), and then heated for 35 min at 60 °C. Subsequently, the suspension fluids were concentrated (9000 r/min, 3 °C, 15 min), and then each supernatant liquid was collected to filter via a 0.22 μm filter membrane. Finally, the filtrates were scanned at 2400 nm/min through a fluorescence spectrometer (F-7100, Hitachi, Japan) with excitation (EX) and emission (EM) wavelengths in the range of 200−600 nm at an interval of 5 nm, for obtaining their spectrograms of three-dimensional excitation−emission matrixes (EEM). Also, the paired-end sequencing of community DNA fragments was revealed through 16S rRNA gene pyrophosphate sequencing to evaluate structural changes in microbial communities. The total DNA was extracted and quantified using the Qubit dsDNA HS. Moreover, the V3 and V4 areas of the 16S rRNA gene were obtained by amplification of 30 ng of DNA as a template where they employed the upstream and downstream primers of ACTCCTACGGGAGGCAGCA and CGGACTACHVGGGTWTCTAAT, respectively. After completing these gene sequence tests, the amplified products were purged and reclaimed by small magnetic beads and quantified by fluorescence with a microplate reader (BioTek, FLx800, Agilent, America). Finally, high-throughput sequencing and gene libraries were prepared using the Illumina TruSeq Nano DNA LT Library Prep Kit.[26]

2.7. Analysis of Variance and Kinetic Modeling. To investigate whether the effects of $NiCo_2O_4$ NPs added in the DF on the amount of bioH_2 was statistically significant, the average with standard deviations of the three parallel experiments were calculated and analyzed by one-way ANOVA using Origin 2021 software to calculate P values, where $P < 0.05$ was significant. The average values were fitted by the modified Gomperz model (eq 1) for evaluating the kinetic process of H_2 generation via DF. Thus, the kinetic values such as the lag phase, maximum H_2 yield, and maximum H_2 production rate (HPR) were used to evaluate the correlation coefficient (R^2).[18]

$$P(t) = Pm \exp\left\{-\exp\left[\frac{R_m \times e}{P_m}(\lambda - t) + 1\right]\right\} \quad (1)$$

https://doi.org/10.1021/acsomega.2c05580
ACS Omega 2022, 7, 41594−41605

where t (h) = DF time, $P(t)$ = H_2 yield (mL/g glucose), P_m = maximum H_2 yield (mL/g glucose), e = 2.72, R_m = maximum HPR (mL/g glucose·h), and λ = lag phase (h).

3. RESULTS AND DISCUSSION

3.1. Characterization of $NiCo_2O_4$ NPs. The morphology, crystal texture, elemental composition, and surface area were detected to explore the effect of $NiCo_2O_4$ NPs on H_2 generation on DF, which are revealed in Figure 1.

In Figure 1a, the XRD spectra revealed the typical spinel structure: diffraction peaks at 2θ = 18.9, 31.1, 36.6, 38.4, 44.6, 53.8, 59.0, and 64.9° corresponded to the characteristic peaks of the standard spectrum of Joint Committee on Powder Diffraction Standards (JCPDS) with card number 20−0781. Also, there were no impurity peaks in the XRD spectra as a whole, which indicated the high purity of the prepared material. In addition, the narrow and sharp diffraction peaks illustrated that the $NiCo_2O_4$ NPs had a high proportion of crystalline regions, thus making the material less susceptible to damage.[28,29] In addition, Figure 1b describes the EDS pattern; the mass percentages of Ni, Co, and O were 12.9, 62.8, and 19.0% respectively. Figure 1c exhibits the SEM images of $NiCo_2O_4$ NPs with a 20,000 magnification, which showed the appearance with a polyhedral shape. In addition, the particles were relatively uniform and smooth, where $NiCo_2O_4$ NPs were slightly agglomerated due to van der Waals forces.[30] The elemental mapping (Figure 1d−h) revealed the distribution of Ni, Co, O, and C. Moreover, the BET surface area of $NiCo_2O_4$ NPs was 12.4249 m^2/g, and the average pore diameter for adsorption and desorption was between 1 and 14 nm (Table 2).

Table 2. BET Test Data of $NiCo_2O_4$ NPs

	item	data
surface area	BET surface area	12.4249 m^2/g
pore size	adsorption average pore diameter (4 V/A by BET)	13.2636 nm
	desorption average pore diameter (4 V/A by BET)	1.7022 nm

Furthermore, the XPS technique was used to acquire the elemental composition and chemical bonds of $NiCo_2O_4$ NPs. Figure 2a reveals the full spectrum map of $NiCo_2O_4$ NPs and demonstrates the existence of Ni, Co, and O. This was not only consistent with the XRD characterization but also indicated the high purity of the $NiCo_2O_4$ NPs.

The existence of element C in the sample was the corollary of the material preparation when XPS analysis was performed. The orbital peaks at 529, 780, and 855 eV confirmed the presence of O 1s, Co 2p3, and Ni 2p3, respectively. The curves of O 1s revealed different oxygen components and were labeled as O 1 and O 2, respectively (Figure 2b). Figure 2b shows that the peak of O 1 corresponded to the typical metal−oxygen bond in the oxide and the binding energy value was 529.6 eV, while the O 2 peak at 530.9 eV was oxygen vacancies.[31,32] The vacancies play part in mitigating the resistance of H^+ movement and accelerating its shuttling in the surface layer.[33] The Ni 2p profiles with two peaks at 855.2 and 872.3 eV for 2p2/3 and 2p1/3, respectively, indicate the existence of Ni^{2+} (Figure 2c). The peak at 860.5 eV ascribed the appearance of Ni^{3+}, and the peak at 879.8 eV was the coexistence of Ni^{2+} and Ni^{3+}.[34] The profile of Co 2p exhibited two peaks of 2p3/2 and 2p1/2 at 780.1 and 795.5 eV, respectively, which signified the existence of Co^{3+} (Figure 2d). Meanwhile, the satellite peaks at 783.2 and 802.9 eV demonstrated the presence of Co^{2+}.[35]

3.2. Effect of $NiCo_2O_4$ NPs on $bioH_2$ Yield. The influences of $NiCo_2O_4$ NPs at seven dosage levels on the $bioH_2$ generation by DF are depicted in Figure 3, where Figure 3a shows the variation of H_2 yield with DF time and Figure 3b represents the HPR.

It can be found that H_2 synthesis started at the 9th hour and almost completely ended at the 24th hour. The moderate amount of $NiCo_2O_4$ NPs (400 mg/L) could facilitate $bioH_2$ generation, and the largest H_2 production of 259.67 mL/g glucose was reached at the addition of 400 mg/L, which increased by 33.97%, matching with the control yield (193.82 mL/g glucose). Table 3 provides the increased value of different materials on the total $bioH_2$ yield when DF was performed with glucose as substrate, indicating that this experiment was at a higher level of $bioH_2$ synthesis.[21,24,25,36]

Cao et al.[21] used alkali-based magnetic nanosheets (AMNSs) (100 mg/L) to increase H_2 yield via DF and obtained the highest yield of 232.8 mL/g glucose, being lower than that (259.67 mL/g glucose) from this work.[21] Similarly, Sun et al.[25] obtained the largest H_2 yield of 272.2 mL/g glucose amended by 400 mg/L manganese ferrite NPs, which was slightly higher than that of this study.[25] Moreover, NPs entered the cell and increase intracellular ET, thereby accelerating the synthesis of $bioH_2$.[36] Nonetheless, there are still some difficulties in comparison to the H_2 yields, mainly due to their different additives and anaerobes in DF systems. A previous work reported that NPs may attach to bacteria and interact with structural proteins on the membrane in $bioH_2$ synthesis via DF.[21,36] A further increase in $NiCo_2O_4$ NPs (more than 400 mg/L) resulted in a decrease in H_2 yield. The production of H_2 was 188.14 mL/g glucose when the dosage of $NiCo_2O_4$ NPs up to 800 mg/L, which reduced to 97% of the control yield. A study about DF utilizing potato peel as substrate had similarly concluded that excess Fe_3O_4 NPs led to the death of anaerobes due to oxidative stress.[37] Other studies showed that cell membranes acted as transport channels for metal ions, but excess metal ions could lead to impaired membrane due to problems with protein. The above reasons inhibit the activity of microbial and even lead to their death, likely causing a decline in the H_2 yield when the dosage of $NiCo_2O_4$ NPs exceeded 400 mg/L. Figure 3b reveals the variation of HPR with DF time. The trend of HPR over time was approximately the same in all groups, with $bioH_2$ synthesis after the 9th hour and peak period at 12−15 h. The highest HPR value of all DF groups was 48.74 mL/g/h and reached 400 mg/L $NiCo_2O_4$ NPs, which was increased by 64.77% with the control HPR (29.58 mL/g/h), providing evidence for the ability of $NiCo_2O_4$ NPs to promote DF for H_2 yield.

3.3. Dynamical Analysis and Mathematical Statistics. The H_2 generation via DF was conformed to the modified Gompertz equation; the detailed records are presented in Table 4. The kinetic fitting study illustrated that the lag phase (λ) was between 11 and 12 h for all DF groups, and the maximum H_2 yield and HPR were also in general agreement with the experiment data. In addition, the fitted correlation R^2 was greater than 99%, which not only indicated a successful fit of datas but was also consistent with the results of Figure 3. A slight drop of trend showed in λ with the increasing doses of

https://doi.org/10.1021/acsomega.2c05580
ACS Omega 2022, 7, 41594−41605

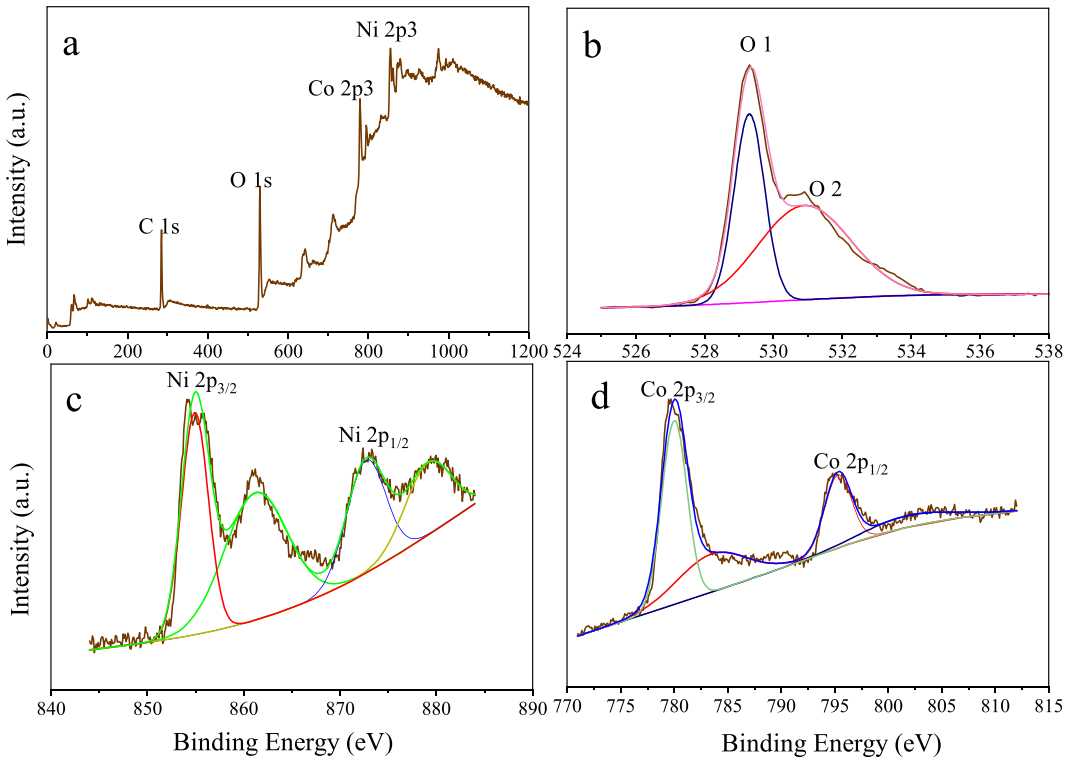

Figure 2. XPS spectrogram of $NiCo_2O_4$ NPs: full spectrogram (a); XPS spectrogram of O 1s (b), XPS spectrogram of Ni 2p (c); XPS spectrogram of Co 2p (d).

$NiCo_2O_4$ NPs, but when $NiCo_2O_4$ NPs outnumbered 400 mg/L, the λ increased instead. Interestingly, even at 400 mg/L of $NiCo_2O_4$ NPs dosing, its λ (11.42 h) was a little greater than that of the control group (11.31 h). This showed that $NiCo_2O_4$ NPs prolonged the DF lag period slightly. Also, this may be related to the inhibition of HPB by $NiCo_2O_4$ NPs at the start of DF, similarly found by Zhang et al.[38] In this study, the lag phase with the highest H_2 yield was 0.11 h longer than that of the control group. Moreover, one-way ANOVA was performed by Origin 2021 software for SMPs, HBu and H_2 yields at seven dosage levels of $NiCo_2O_4$ NPs, and the results are described in Table 5. There was a correlation between $NiCo_2O_4$ NP dosage and SMP, HBu, and H_2 yield, as the *p*-values were all below 0.005. In addition, the final pH values of all DF were between 4.75 and 4.95, reaching the stable pH level at the end of DF (4.8−5.0).[39]

3.4. Impact of $NiCo_2O_4$ NPs on SMPs. To probe the influence of different doses of $NiCo_2O_4$ NPs on the DF, the SMP composition of the zymotic fluid was measured for all groups and the outcomes are exhibited in Figure 3c. The SMPs showed an increasing trend during the DF process with the proper $NiCo_2O_4$ NPs added (0−400 mg/L). When the $NiCo_2O_4$ NPs was injected at 400 mg/L, the SMPs reached the highest level of 5860 mg/L and was a 28.34% increase over the control SMPs (4570 mg/L). Figure 3d supplies the changing trends of glucose decomposition and SMPs yield from the 400 mg/L $NiCo_2O_4$ NPs (the highest H_2 yield group), which changed rapidly during 6−18 h of DF. Whereas, the SMPs decreased to 97.4% when $NiCo_2O_4$ NPs was up to 800 mg/L. Different addition levels proved that $NiCo_2O_4$ NPs promoted the conversion rate of substrate within a certain range (0−400 mg/L), which coincided with H_2 yield. SMPs decreased with increasing $NiCo_2O_4$ NPs (more than 400 mg/L) due to the irreversible damage about organelles and genetic material caused by excessive NPs crossing the cell membrane.[40] The liquid phase products generated by DF were more favorable for H_2 yield when HBu and HAc were predominant. Because the theoretical values of H_2 evolution for different DF pathways were not equal, the theoretical H_2 yields were 4 and 2 mol for 1 mol of glucose through the HAc and HBu metabolic pathways, respectively.[41] As shown in Figure 3c, the HAc and HBu accounted for 26−31% and 58−62% of SMPs, respectively. They were much larger than the sum (10−16%) of HPr and EtOH from the SMPs in all DF groups, proving that the H_2−DF was mainly HBu and HAc pathways.

3.5. Dissolution of $NiCo_2O_4$ NPs and the Effect on EPS. To investigate the effects of the $NiCo_2O_4$ NPs on the DF liquid phases, Ni and Co ions were detected and the outcomes are exhibited in Figure 4. $NiCo_2O_4$ NPs released trace amounts of Co and Ni ions in the H_2−DF process, and their concentrations in DF broth was increased with the addition of $NiCo_2O_4$ NPs. Furthermore, the *p*-values for Ni and Co ions concentration calculated from the one-way ANOVA were not greater than 0.05, which indicated that the dosing of $NiCo_2O_4$ NPs at different levels had an obvious influence on the concentrations of Co and Ni ions in the DF liquid (Table 5). In addition, the Co ions in each group of zymotic fluid are slightly more than twice that of Ni ions, probably owing to the use of Ni^{2+} by the germs. Li et al.[42] demonstrated that microbes utilized the element Ni when shrimp shell biochar loaded with nickel was applied for methanogenesis studies.[42] Moreover, EPS was a gelatinous polymer secreted by microbes that existed outside the cell, and its function was to protect bacteria. The control (0 mg/L), highest (400 mg/L), and lowest (800 mg/L) H_2 yield groups were measured for the

https://doi.org/10.1021/acsomega.2c05580
ACS Omega 2022, 7, 41594−41605

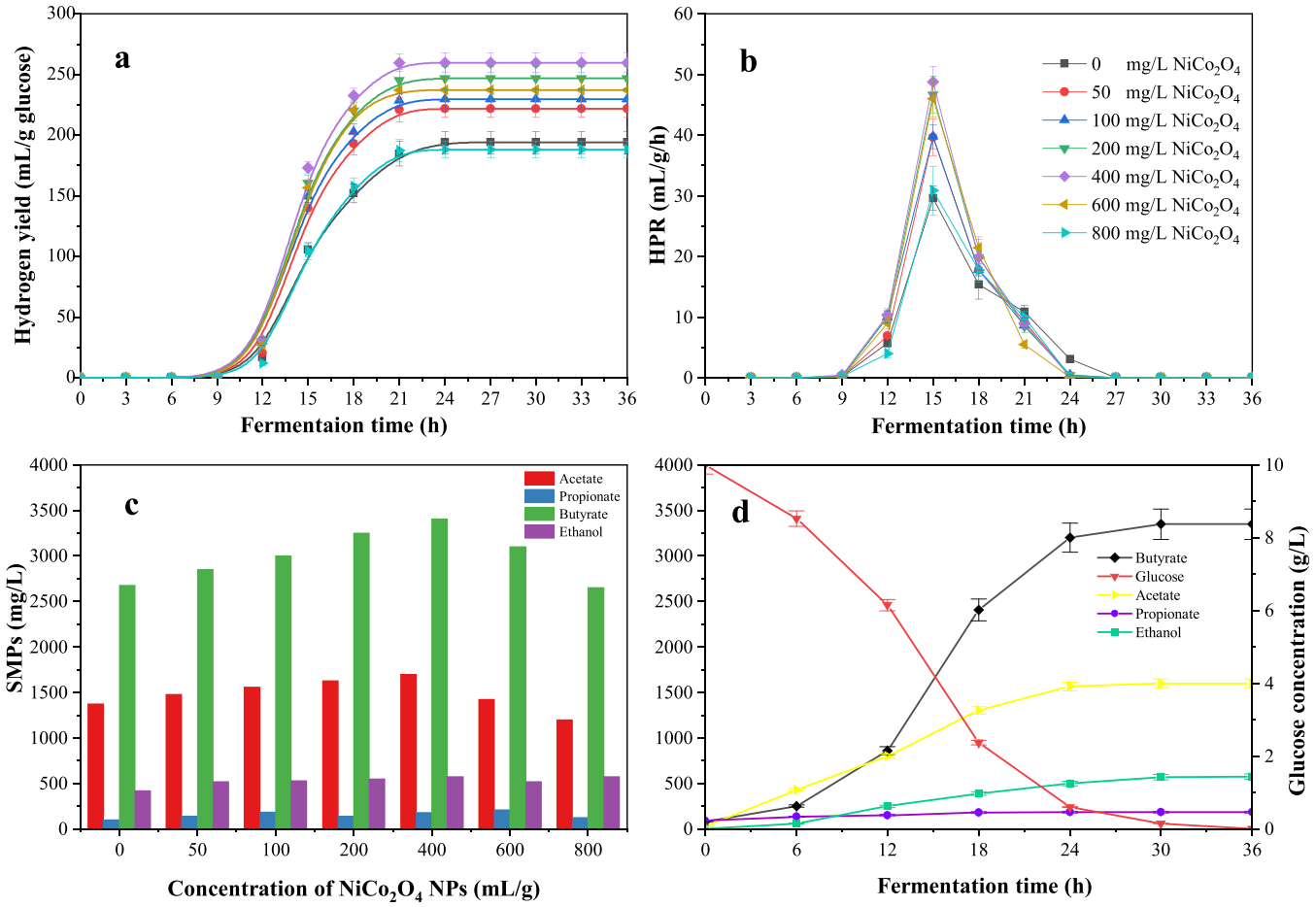

Figure 3. Effect of different doses of $NiCo_2O_4$ NPs on bioH_2 production by DF: (a) bioH_2 yields; (b) rates of bioH_2 yield; (c) effect of different dosages of $NiCo_2O_4$ NPs on SMPs and glucose; (d) change of glucose and SMPs with 400 mg/L $NiCo_2O_4$ NPs.

Table 3. Comparison of H_2 Production by DF under Different Conditions

substrate	inoculum	initial pH/ DF temp.	additives/dosage (mg/L)	H_2 yield(mL/g)	reference
glucose	anaerobic sludge	6.9, 37 °C	AMNSs/100	232.8	Cao et al.[21]
glucose	anaerobic sludge	7.0, 55 °C	AMNSs/400	150.3	Cao et al.[21]
glucose	*C. pasteurianum*	7.0, 35 °C	Fe/50	255.7	Hsieh et al.[24]
glucose	anaerobic sludge	7.0, 37 °C	$MnFe_2O_4$/400	272.7	Sun et al.[25]
glucose	anaerobic sludge	7.0, 37 °C	Fe_3O_4/100	198.30	Sun et al.[36]
glucose	anaerobic sludge	7.0, 37 °C	Fe_3O_4-rGO NCs/100	225.60	Sun et al.[36]
glucose	anaerobic sludge	6.9, 37 °C	$NiCo_2O_4$/400	259.67	this work

Table 4. Kinetic Parameters of bioH_2 by DF and Final pH

$NiCO_2O_4$ (mg/L)	P_m (mL/g)	R_m (mL/(g·h))	λ (h)	R^2 (100%)	final pH
0	194.09	28.94	11.31	99.89	4.81 ± 0.1
50	221.86	41.91	11.65	99.94	4.86 ± 0.1
100	229.95	42.11	11.60	99.96	4.93 ± 0.1
200	247.01	46.69	11.58	99.97	4.81 ± 0.1
400	259.81	50.91	11.42	99.96	4.76 ± 0.1
600	237.56	48.72	11.61	99.99	4.81 ± 0.1
800	188.52	33.54	11.82	99.93	4.95 ± 0.1

Table 5. One-Way ANOVA in all Groups

project	*p*-H_2	*p*-SMPs	*p*-HBu	*p*-Ni ions	*p*-Co ions
value	<0.05	<0.05	<0.05	<0.05	<0.05

identification of fluorescent dissolved organic compounds. Generally, EEM analysis was not precise because it was a semiquantitative technique.[43] The five regions were divided according to the range of excitation (EX) and emission (EM) wavelengths and represented different substances; the specific partition method was referred to previous studies.[18]

In Figure 5, there were no significant differences in the regions of I (tyrosine-like proteins), II (tryptophan-like proteins), and III (fulvic acid-like organics) for three groups, while there were obvious discrepancies in IV (soluble microbial metabolites) and V (humic acid-like). The fluorescence intensity in region IV was evidently stronger in the highest H_2 yield group than that of the others. This agreed with the detection results of SMPs, once more providing new evidence that a moderate amount of $NiCo_2O_4$ NPs (400 mg/L) played vital roles in the utilization of substrate and production of SMPs. Region V represented humic acid-like,

https://doi.org/10.1021/acsomega.2c05580
ACS Omega 2022, 7, 41594−41605

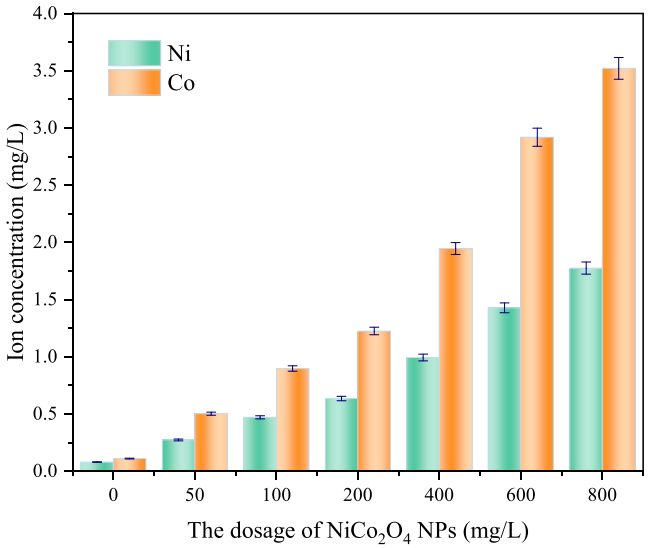

Figure 4. Ni and Co ion concentrations in the final fermentation broth of each group.

whose structure included an amount of oxygen-containing functional groups that were difficult to biodegrade.[44] Although its distribution on the outside of the cell played a role in protecting microbes, at high concentrations, it can also lead to a hindrance in the uptake of nutrients by the germs, as its gelatinous nature leads to an increase in viscosity on the outside of the cell.[35] Furthermore, humic acid-like can also cause changes in the enzyme particle size and the structure of amino acids by binding to biological enzymes, thereby loosening the structure of protease and reducing its activity.[45] Some metal ions can mitigate the inhibition of polysaccharides and relate enzymes by complexing with humic acid-like.[46] The intensity of mitigation is related to the type and concentration of metal ions, and the alleviating of humic acid-like by bimetallic ions can obtain a synergistic effect of 1 + 1 > 2.[47] The fluorescence responses of the control and the lowest H_2 yield groups were not significantly different in region V, but they responded more strongly than that of the highest H_2 yield DF group. This phenomenon was attributed to the better complexation of dissolved Ni^{2+} and Co^{3+} with humic acid-like via electrostatic force, cation exchange, and sweep flocculation in the DF reactor with 400 mg/L of $NiCo_2O_4$ NPs (the highest H_2 yield), resulting in the reduced fluorescence intensity in region V (humic acid-like). This suggested that the moderate amounts of $NiCo_2O_4$ NPs could reduce humic acid-like. This was obviously favorable to high H_2 yield, and the reason may be the shielding effects of Ni and Co ions released from $NiCo_2O_4$ NPs. While the enhanced fluorescence intensity of the lowest H_2 yield group was likely attributed to the excessive release of Ni and Co ions from DF broth, the strong mutual repulsion between positive charges could hinder the mutual binding between metal ions and humic acid. Li et al.[47] proved that the shielding effect on humic acid decreased with increasing Ca^{2+} and Al^{3+} at dosages higher than 100 and 70 mg/L, respectively.[47]

3.6. Effect of $NiCo_2O_4$ NPs on Microorganisms. Since different bacteria have different tolerance toward $NiCo_2O_4$ NPs, the fermented sludge from the control group (0 mg/L), the highest (400 mg/L), and lowest (800 mg/L) H_2 groups was taken for a microbiological assay by 16S rRNA gene sequencing technology.[48] The reliability of the sequencing was confirmed by the valid sequence numbers of the three samples ranging from 70,400 to 76,684, and the good coverage were 0.999 in all cases. In addition, the Shannon index of germs in DF systems with 0, 400, and 800 mg/L $NiCo_2O_4$ NPs dosages were 6.31099, 6.00387, and 5.93574, respectively. This result corroborated that $NiCo_2O_4$ NPs reduced the microbial diversity because the Shannon index represented the level of biodiversity and they were positively correlated. Analogous phenomena were investigated by Zhang et al.[14] who concluded that the Shannon indexes that matched with control samples in mesophilic and thermophilic conditions were decreased by 0.338 and 0.036, respectively.[14] Figure 6 illustrates the microbial profile of the three samples at the phylum and genus levels.

The *Firmicutes*' abundance was absolutely dominant in the grade of phylum (Figure 6a), which could form spores to resist harsh environments in very short periods, and break down substrates to obtain H_2.[49] The abundance of *Firmicutes* in the highest H_2 yield group (400 mg/L, 84.04%) increased by 6.61% comparing with the control group (0 mg/L, 77.43%). Meanwhile, the relative abundance of *Firmicutes* in the lowest H_2 yield group (800 mg/L, 74.90%) was reduced by 2.53%, matching the control abundance. A homologous phenomenon was that a moderate amount of Fe_3O_4 NPs could heighten the abundance of *Firmicutes* in DF confirmed by previous

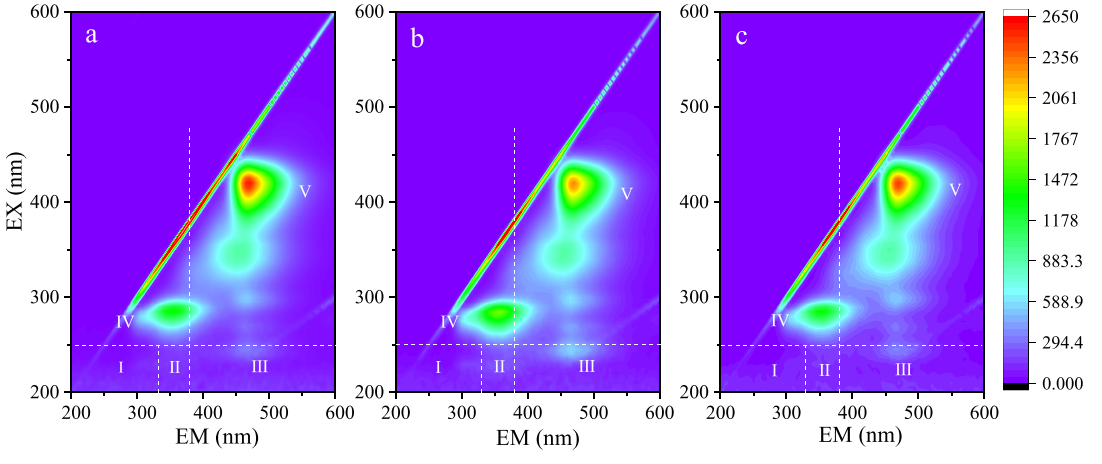

Figure 5. EEM spectra s of EPS from final DF: (a) 0, (b) 400, and (c) 800 mg/L.

https://doi.org/10.1021/acsomega.2c05580
ACS Omega 2022, 7, 41594−41605

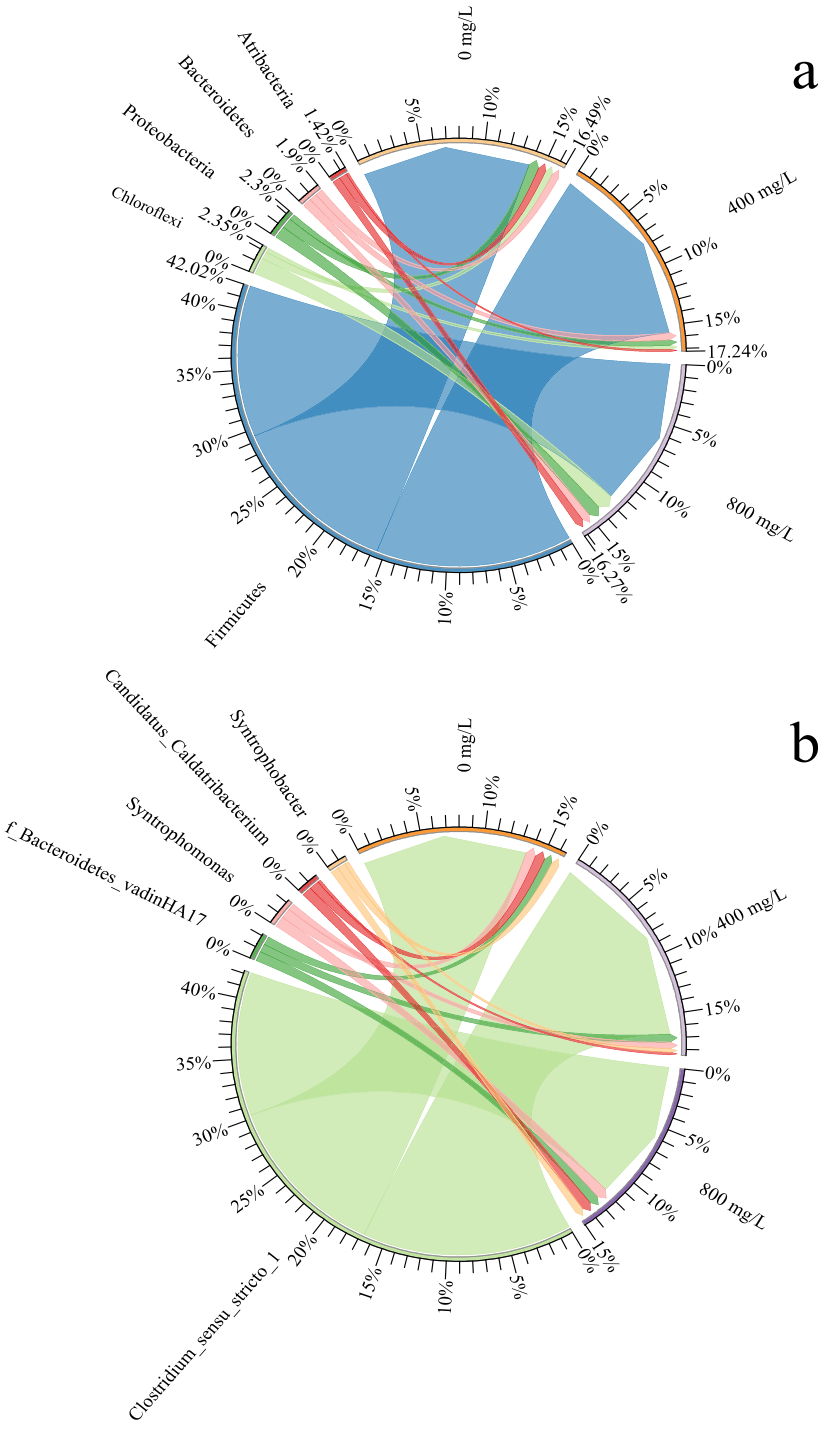

Figure 6. Microbial communities at different $NiCo_2O_4$ NPs additions: (a) phylum; (b) genus (top 5 of the samples).

research.[50] Interestingly, the relative abundance of *Firmicutes* in the previous studies was 35−49 and 29−42%, respectively, with or without the addition of NPs to the H_2−DF system, being much lower than the proportion of *Firmicutes* in this work (74.90−84.04%).[26,35] The reason why *Firmicutes* in this work was much greater than that in the previous two studies was probably due to the better sludge cultured. A similar finding was reported that the more *Firmicutes* in the H_2−DF reactor, the more H_2.[51] The microbial structural distribution at the genus level is described in Figure 6b. *Clostridium sensu stricto1* had absolute predominance, and there were no significant differences in the abundance of other bacteria. The proportions of *Clostridium sensu stricto1* from the highest (400 mg/L, 71.48%) and lowest (800 mg/L, 50.95%) H_2 yield groups were 1.23 and 0.88 times higher than that of the control (58.08%), respectively. H_2 yield was positively correlated with *Clostridium sensu stricto1*, being attributed to the fact that such bacteria could convert glucose into H_2.[52] In addition, *Clostridium sensu stricto1* pertained to *Firmicutes*, agreeing with the changes of microbial assays at the phylum level.[53]

Moreover, the effect of $NiCo_2O_4$ NPs on the microbes in the H_2−DF system at the species level was demonstrated in Figure7a. It can be seen that *Clostridium butyricum* (*C. butyricum*) was absolutely dominant. The relative abundance of

https://doi.org/10.1021/acsomega.2c05580
ACS Omega 2022, 7, 41594−41605

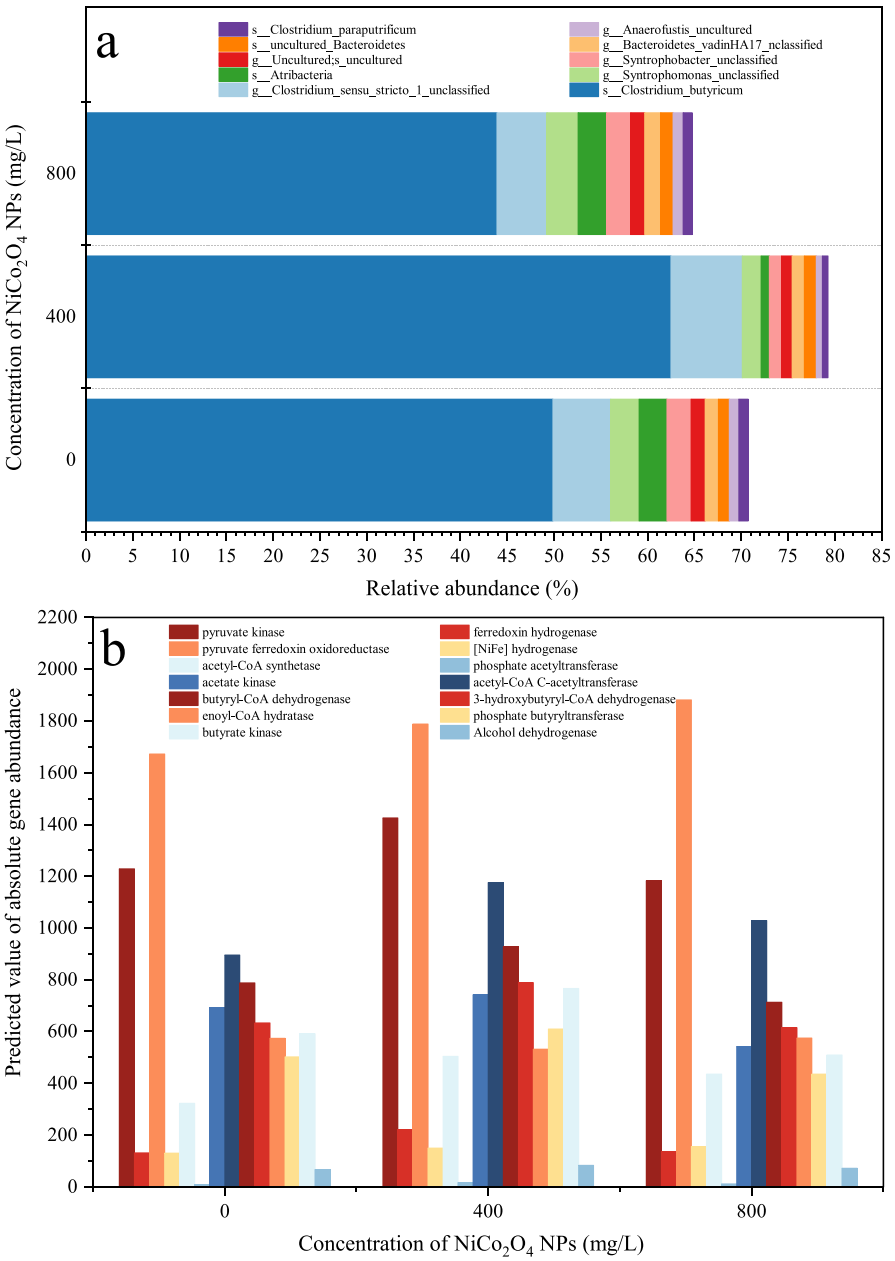

Figure 7. (a) Relative abundance of microbial species levels under different $NiCo_2O_4$ NPs addition conditions; (b) Predicted abundance of genes encoding key enzymes in different $NiCo_2O_4$ NPs addition groups.

C. butyricum corresponding to the $NiCo_2O_4$ NPs supplemented with 0, 400, and 800 mg/L were 49.88, 62.51, and 43.90%, respectively. The *C. butyricum* of the latter two groups increased by 25.32% and decreased by 11.99% compared with the control sample. A moderate amount (400 mg/L) of $NiCo_2O_4$ NPs was instrumental in the multiplication of *C. butyricum*, while excess $NiCo_2O_4$ NPs led to the opposite result. These phenomena accorded with the microbial structure in genus levels. The *C. butyricum* is a typical dominant microbe in the HBu pathway of H_2−DF. Fu et al.[54] also illustrated that Raney nickel, nickel, and copper particles contribute to its growth and reproduction.[54] This study confirmed that appropriate dosing of $NiCo_2O_4$ NPs (400 mg/L) promoted that the reproduction of *C. butyricum* dominated in *Clostridium sensu stricto1*, thereby facilitating the HBu−DF for more bioH_2. However, a decrease in *C. butyricum* was revealed when the dose of $NiCo_2O_4$ NPs was greater than 400 mg/L, which was consistent with the total amount of SMPs and H_2.

3.7. Predicted Functional Analysis of Genes in HPB.

For further comprehension of the pathways of substrate transformation by bacterial communities in DF systems, the 16S rRNA gene sequences of the microbial genome were compared with those of the Kyoto Encyclopedia of Genes and Genomes (KEGG) by PICRUSt software. Also, the predicted absolute abundance of key genes is exhibited in Figure 7b. Genetic predictions indicated that the DF processes enriched for gene expression that converted glucose to phosphoenolpyruvate: pyruvate kinase, the rate-limiting enzyme in the glycolytic phase.[18] The H_2−DF groups with $NiCo_2O_4$ NPs of 400 and 800 mg/L, elevated by 16.1% and reduced by 3.8%, respectively, compared with the control sample, indicating that

https://doi.org/10.1021/acsomega.2c05580
ACS Omega 2022, 7, 41594−41605

adequate addition (400 mg/L) of $NiCo_2O_4$ NPs was profitable to the glycolytic process. More importantly, most of the H_2 in the DF process is generated under the catalysis of ferredoxin hydrogenase: 2 H^+ + 2 reduced ferredoxins < = > 2 oxidized ferredoxins + H_2, which are the most significant H_2-producing enzymes.[55] In this work, the predicted absolute abundance of the gene encoding ferredoxin hydrogenase in the group of 400 mg/L $NiCo_2O_4$ NPs added was enhanced by 68.7% of the control one, but there was no obvious variation in the group supplemented with 800 mg/L $NiCo_2O_4$ NPs. In addition, pyruvate ferredoxin oxidoreductase participates in the reaction: 2 oxidized ferredoxin + CoA + pyruvate = 2 reduced ferredoxin + acetyl-CoA +2 H^+ + CO_2. The reduced ferredoxin catalyzes the proton to H_2 by hydrogenase or ferredoxin hydrogenase. Interestingly, the predicted genes abundance of encoding pyruvate ferredoxin oxidoreductase and [Fe−Ni] hydrogenase in this work increased with the increasing doses of $NiCo_2O_4$ NPs and both being the highest at the dose of 800 mg/L, with an enhancement of 12.5 and 19.8% over the control, respectively. Gene prediction results proved that 400 mg/L of $NiCo_2O_4$ NPs in H_2−DF increased the abundance of genes encoding glycolytic processes and other enzymes related to H_2 yield. In addition, the predicted levels of genes encoding acetyl−CoA synthetase, acetate kinase, butyrate kinase, etc., were elevated to varying degrees when 400 mg/L $NiCo_2O_4$ NPs were added. This was in line with the changes of the SMP assay. In addition, the common strains in the DF-H_2 generation pathway with HAc and HBu as products all belong to *Clostridium*, being in line with the results of the detection of microbes in this work.[21,56−58]

3.8. Mechanism of BioH$_2$ Yield Improvement. The mechanisms of NPs in bioH_2 production through DF in former works are summarized as follows: (a) optimizing microbial community structure; (b) changing EPS; (c) accelerating ET. Furthermore, Zhang et al.[14] and Li et al.[59] uncovered that NPs could attach to bacteria and interact with structural proteins on the membrane in a work about DF.[14,59] In this work, more detailed probable H_2 enhancing mechanisms were proposed: (a) By virtue of the QSE and HSA of $NiCo_2O_4$ NPs, not only the rate of ET between HPB can be accelerated but also the synthesis of hydrogenases. (b) Ni participates in the synthesis of [Fe−Ni] hydrogenase and acetyl−CoA synthase. The former facilitates the catalytic reduction of protons to H_2, while the latter is a key intermediate in the yield of SMPs. (c) $NiCo_2O_4$ NPs can adhere to the cell surface or enter the cell, thus facilitating the ET process. (d) The Co and Ni ions released by $NiCo_2O_4$ NPs provide HPB with important trace elements required for multiplying, thus optimizing the community structure of bacteria. (e) Ni and Co ions released from $NiCo_2O_4$ NPs relieved the inhibitory effect of humic acid-like. (f) $NiCo_2O_4$ NPs promoted the expression of key genes in the DF process.

4. CONCLUSIONS

$NiCo_2O_4$ NPs was prepared to improve the H_2 productivity by DF. The highest H_2 production (259.67 mL/g glucose) was achieved at the $NiCo_2O_4$ NPs supplemented with 400 mg/L, which was enhanced by 33.97% compared to the control sample (193.82 mL/g glucose). In addition, the relative abundance of *C. butyricum* increased by 25.32%, promoting the HBu pathway. The inhibitory effect of humic acid-like in H_2−DF was effectively alleviated. Gene predictions indicated that the abundance of genes encoding key enzymes related to H_2 synthesis were enhanced by $NiCo_2O_4$. This work provides a theoretical basis for the achieve energy recovery of DF treating food processing wastewater.

AUTHOR INFORMATION

Corresponding Author

Jishi Zhang − *College of Environmental Science and Engineering, Qilu University of Technology (Shandong Academy of Sciences), Jinan 250353, China;* orcid.org/0000-0003-0054-2726; Email: lyzhangjishi@163.com

Authors

Zhenmin Li − *College of Environmental Science and Engineering, Qilu University of Technology (Shandong Academy of Sciences), Jinan 250353, China*

Jiangmei Wang − *Shandong Weifang Ecological Environment Monitoring Center, Weifang 261041, China*

Kexin Tian − *College of Environmental Science and Engineering, Qilu University of Technology (Shandong Academy of Sciences), Jinan 250353, China*

Chen Zhou − *College of Environmental Science and Engineering, Qilu University of Technology (Shandong Academy of Sciences), Jinan 250353, China*

Yong Pei − *College of Environmental Science and Engineering, Qilu University of Technology (Shandong Academy of Sciences), Jinan 250353, China*

Lihua Zang − *College of Environmental Science and Engineering, Qilu University of Technology (Shandong Academy of Sciences), Jinan 250353, China*

Complete contact information is available at: https://pubs.acs.org/10.1021/acsomega.2c05580

Author Contributions

Z.L: investigation, writing and editing, visualization, and methodology;J.W: writing and methodology; K.T: review and editing; C.Z: formal analysis and data curation; Y.P: formal analysis; J.Z: conceptualization, review and editing, funding acquisition and Supervision; L.Z: project administration.

Notes

The authors declare no competing financial interest.

ACKNOWLEDGMENTS

This work is funded by the Natural Science Foundation of Shandong Province (ZR2016EEM33) and the Foundation (ZZ20210125) of State Key Laboratory of Biobased Material and Green Papermaking, China.

REFERENCES

(1) Cai, Z.; Zhang, W.; Zhang, J.; Zhang, J.; Ji, D.; Gao, W. Effect of ammoniated fiber explosion combined with H_2O_2 pretreatment on the hydrogen production capacity of herbaceous and woody waste. *ACS Omega* **2022**, *7*, 21433−21443.

(2) Sudakov, I.; Vakulenko, S. A.; Bruun, J. T. Stochastic physics of species extinctions in a large population. *Phys. A* **2022**, *585*, 126422.

(3) Mok, P. L. H.; Antonsen, S.; Agerbo, E.; Brandt, J.; Geels, C.; Christensen, J. H.; Frohn, L. M.; Pedersen, C. B.; Webb, R. T. Exposure to ambient air pollution during childhood and subsequent risk of self−harm: A national cohort study. *Prev. Med.* **2021**, *152*, 106502.

(4) Zhang, J.; Yao, C.; Fan, C. Enhancement of Solubility and Biohydrogen Production from Sewage Sludge with Lime Mud Filtrate. *Water Air Soil Poll.* **2018**, *229*, 129.

(5) Yan, X.; Li, Y.; Sun, C.; Zhang, C.; Yang, L.; Fan, X.; Chu, L. Enhanced H_2 production from steam gasification of biomass by red

https://doi.org/10.1021/acsomega.2c05580
ACS Omega 2022, 7, 41594−41605

mud−doped Ca−Al−Ce bi−functional material. *Appl. Energy* **2022**, *312*, 118737.
(6) Chen, Y.; Lan, L.; Hao, Z.; Fu, P. Cradle−grave energy consumption, greenhouse gas and acidification emissions in current and future fuel cell vehicles: Study based on five hydrogen production methods in China. *Energy Rep.* **2022**, *8*, 7931−7944.
(7) Laurinavichene, T.; Belokopytov, B. F.; Laurinavichius, K. S.; Tekucheva, D. N.; Seibert, M.; Tsygankov, A. A. Towards the integration of dark−and photo−fermentative waste treatment. 3. Potato as substrate for sequential dark fermentation and light−driven H_2 production. *Int. J. Hydrogen Energy* **2010**, *35*, 8536−8543.
(8) Pandey, A.; Sinha, P.; Pandey, A. Hydrogen production by sequential dark and photofermentation using wet biomass hydrolysate of Spirulina platensis: Response surface methodological approach. *Int. J. Hydrogen Energy* **2021**, *46*, 7137−7146.
(9) Rahman, S. N. A.; Masdar, M. S.; Rosli, M. I.; Majlan, E. H.; Husaini, T.; Kamarudin, S. K.; Daud, W. R. W. Overview biohydrogen technologies and application in fuel cell technology. *Renew. Sustainable Energy Rev.* **2016**, *66*, 137−162.
(10) Sydney, E. B.; Duarte, E. R.; Martinez Burgos, W. J.; de Carvalho, J. C.; Larroche, C.; Soccol, C. R. Development of short chain fatty acid−based artificial neuron network tools applied to biohydrogen production. *Int. J. Hydrogen Energy* **2020**, *45*, 5175−5181.
(11) Kumar, G.; Mathimani, T.; Rene, E. R.; Pugazhendhi, A. Application of nanotechnology in dark fermentation for enhanced biohydrogen production using inorganic nanoparticles. *Int. J. Hydrogen Energy* **2019**, *44*, 13106−13113.
(12) Cheng, J.; Li, H.; Ding, L.; Zhou, J.; Song, W.; Li, Y. Y.; Lin, R. Improving hydrogen and methane co−generation in cascading dark fermentation and anaerobic digestion: The effect of magnetite nanoparticles on microbial electron transfer and syntrophism. *Chem. Eng. J.* **2020**, *397*, 125394.
(13) Rambabu, K.; Bharath, G.; Thanigaivelan, A.; Das, D. B.; Show, P. L.; Banat, F. Augmented biohydrogen production from rice mill wastewater through nano−metal oxides assisted dark fermentation. *Bioresour. Technol.* **2021**, *319*, 124243.
(14) Zhang, J.; Zhao, W.; Yang, J.; Li, Z.; Zhang, J.; Zang, L. Comparison of mesophilic and thermophilic dark fermentation with nickel ferrite nanoparticles supplementation for biohydrogen production. *Bioresour. Technol.* **2021**, *329*, 124853.
(15) Taherdanak, M.; Zilouei, H.; Karimi, K. The effects of Fe^0 and Ni^0 nanoparticles versus Fe^{2+} and Ni^{2+} ions on dark hydrogen fermentation. *Int. J. Hydrogen Energy* **2016**, *41*, 167−173.
(16) Pobeheim, H.; Munk, B.; Lindorfer, H.; Guebitz, G. M. Impact of nickel and cobalt on biogas production and process stability during semi−continuous anaerobic fermentation of a model substrate for maize silage. *Water Res.* **2011**, *45*, 781−787.
(17) Zhang, Q.; Xu, S.; Li, Y.; Ding, P.; Zhang, Y.; Zhao, P. Green−synthesized nickel oxide nanoparticles enhances biohydrogen production of Klebsiella sp. WL1316 using lignocellulosic hydrolysate and its regulatory mechanism. *Fuel* **2021**, *305*, 121585.
(18) Yang, J.; Zhang, H.; Liu, H.; Zhang, J.; Pei, Y.; Zang, L. Unraveling the roles of lanthanum−iron oxide nanoparticles in biohydrogen production. *Bioresour. Technol.* **2022**, *351*, 127027.
(19) Birrell, J. A.; Rodríguez Macia, P.; Reijerse, E. J.; Martini, M. A.; Lubitz, W. The catalytic cycle of [FeFe] hydrogenase: A tale of two sites. *Coord. Chem. Rev.* **2021**, *449*, 214191.
(20) Mullai, P.; Yogeswari, M. K.; Sridevi, K. Optimisation and enhancement of biohydrogen production using nickel nanoparticles−A novel approach. *Bioresour. Technol.* **2013**, *141*, 212−219.
(21) Cao, X.; Zhao, L.; Dong, W.; Mo, H.; Ba, T.; Li, T.; Guan, D.; Zhao, W.; Wang, N.; Ma, Z.; Zang, L. Revealing the mechanisms of alkali−based magnetic nanosheets enhanced hydrogen production from dark fermentation: Comparison between mesophilic and thermophilic conditions. *Bioresour. Technol.* **2022**, *343*, 126141.
(22) Elreedy, A.; Ibrahim, E.; Hassan, N.; El Dissouky, A.; Fujii, M.; Yoshimura, C.; Tawfik, A. Nickel−graphene nanocomposite as a novel supplement for enhancement of biohydrogen production from industrial wastewater containing mono−ethylene glycol. *Energy Convers. Manage.* **2017**, *140*, 133−144.
(23) Beckers, L.; Hiligsmann, S.; Lambert, S. D.; Heinrichs, B.; Thonart, P. Improving effect of metal and oxide nanoparticles encapsulated in porous silica on fermentative biohydrogen production by Clostridium butyricum. *Bioresour. Technol.* **2013**, *133*, 109−117.
(24) Hsieh, P. H.; Lai, Y. C.; Chen, K. Y.; Hung, C. H. Explore the possible effect of TiO_2 and magnetic hematite nanoparticle addition on biohydrogen production by *Clostridium pasteurianum* based on gene expression measurements. *Int. J. Hydrogen Energy* **2016**, *41*, 21685−21691.
(25) Sun, H.; Shen, J.; Hu, M.; Zhang, J.; Cai, Z.; Zang, L.; Zhang, F.; Ji, D. Manganese ferrite nanoparticles enhanced biohydrogen production from mesophilic and thermophilic dark fermentation. *Energy Rep.* **2021**, *7*, 6234−6245.
(26) Li, W.; Zhang, J.; Yang, J.; Zhang, J.; Li, Z.; Yang, Y.; Zang, L. Comparison of copper and aluminum doped cobalt ferrate nanoparticles for improving biohydrogen production. *Bioresour. Technol.* **2022**, *343*, 126078.
(27) Wang, L.; Yuan, L.; Li, Z. H.; Zhang, X.; Leung, K. M. Y.; Sheng, G. P. Extracellular polymeric substances (EPS) associated extracellular antibiotic resistance genes in activated sludge along the AAO process: Distribution and microbial secretors. *Sci. Total Environ.* **2022**, *816*, 151575.
(28) Nakate, U. T.; Kale, S. N. Microwave assisted synthesis and characterizations of $NiCo_2O_4$ nanoplates and Electrical, magnetic properties. *Mater. Today: Proc.* **2016**, *3*, 1992−1998.
(29) Bashir, A.; Shukla, S.; Bashir, R.; Patidar, R.; Bruno, A.; Gupta, D.; Satti, M. S.; Akhter, Z. Low temperature, solution processed spinel $NiCo_2O_4$ nanoparticles as efficient hole transporting material for mesoscopic n−i−p perovskite solar cells. *Sol. Energy* **2020**, *196*, 367−378.
(30) Alsarraf, J.; Al-Rashed, A. A. A. A.; Alnaqi, A. A.; Shahsavar Goldanlou, A. Dominance of cohesion of EG−water molecules over Van der Waals force between SiO_2−ZnO nanoparticles in the liquid interface. *Powder Technol.* **2021**, *379*, 537−546.
(31) Liang, H.; Xu, M.; Bu, Y.; Chen, B.; Zhang, Y.; Fu, Y.; Xu, X.; Zhang, J. Confined interlayer water enhances solid lubrication performances of graphene oxide films with optimized oxygen functional groups. *Appl. Surf. Sci.* **2019**, *485*, 64−69.
(32) Nadargi, D. Y.; Shinde, K. P.; Tamboli, M. S.; Kodam, P. M.; Ghadage, A. V.; Tam Nguyen Truong, N.; Park, J. S.; Suryavanshi, S. S. Enhanced pseudocapacitive properties of divalent (Mn, Fe, Zn) substituted $NiCo_2O_4$ nanorods. *Inorg. Chem. Commun.* **2022**, *143*, 109725.
(33) Luo, Q.; Zhao, Y.; Sun, L.; Wang, C.; Xin, H.; Song, J.; Li, D.; Ma, F. Interface oxygen vacancy enhanced alkaline hydrogen evolution activity of cobalt−iron phosphide/CeO_2 hollow nanorods. *Chem. Eng. J.* **2022**, *437*, 135376.
(34) Guo, W.; Chai, D. F.; Li, J.; Lv, J.; Wang, J.; Guo, D.; Sui, G.; Xing, J. Oxygen vacancy rich and phosphate ions modulated hierarchical mesoporous $NiCo_2O_4$−CoO hollow nanocubes as efficient and stable electrodes for high−performance supercapacitor. *J. Energy Storage* **2022**, *52*, 104849.
(35) Zhang, J.; Li, W.; Yang, J.; Li, Z.; Zhang, J.; Zhao, W.; Zang, L. Cobalt ferrate nanoparticles improved dark fermentation for hydrogen evolution. *J. Cleaner Prod.* **2021**, *316*, 128275.
(36) Sun, Y.; Ma, Y.; Zhang, B.; Sun, H.; Wang, N.; Wang, L.; Zhang, J.; Xue, R. Comparison of magnetite/reduced graphene oxide nanocomposites and magnetite nanoparticles on enhancing hydrogen production in dark fermentation. *Int. J. Hydrogen Energy* **2022**, *47*, 22359−22370.
(37) Singhvi, M.; Maharjan, A.; Thapa, A.; Jun, H. B.; Soo Kim, B. Nanoparticle−associated single step hydrogen fermentation for the conversion of starch potato waste biomass by thermophilic Parageobacillus thermoglucosidasius. *Bioresour. Technol.* **2021**, *337*, 125490.
(38) Zhang, J.; Zhao, W.; Yang, J.; Li, Z.; Zhang, J.; Zang, L. Comparison of Mesophilic and Thermophilic Dark Fermentation

https://doi.org/10.1021/acsomega.2c05580
ACS Omega 2022, 7, 41594−41605

With Nickel Ferrite Nanoparticles Supplementation for Biohydrogen Production. *Bioresour. Technol.* **2021**, *329*, 124853.
(39) Zhao, W.; Zhang, J.; Zhang, H.; Yang, M.; Zang, L. Comparison of Mesophilic and Thermophilic Biohydrogen Production Amended by Nickel−Doped Magnetic Carbon. *J. Cleaner Prod.* **2020**, *270*, 122730.
(40) Burketová, L.; Martinec, J.; Siegel, J.; Macůrková, A.; Maryška, L.; Valentová, O. Noble metal nanoparticles in agriculture: impacts on plants, associated microorganisms, and biotechnological practices. *Biotechnol. Adv.* **2022**, *58*, 107929.
(41) Cai, G.; Jin, B.; Monis, P.; Saint, C. Metabolic flux network and analysis of fermentative hydrogen production. *Biotechnol. Adv.* **2011**, *29*, 375−387.
(42) Li, X.; Wu, M.; Xue, Y. Nickel−loaded shrimp shell biochar enhances batch anaerobic digestion of food waste. *Bioresour. Technol.* **2022**, *352*, 127092.
(43) Maqbool, T.; Ly, Q. V.; Asif, M. B.; Ng, H. Y.; Zhang, Z. Fate and role of fluorescence moieties in extracellular polymeric substances during biological wastewater treatment: A review. *Sci. Total Environ.* **2020**, *718*, 137291.
(44) Ryu, J.; Jung, J.; Park, K.; Song, W.; Choi, B.; Kweon, J. Humic acid removal and microbial community function in membrane bioreactor. *J. Hazard. Mater.* **2021**, *417*, 126088.
(45) Liang, T.; Elmaadawy, K.; Liu, B.; Hu, J.; Hou, H.; Yang, J. Anaerobic fermentation of waste activated sludge for volatile fatty acid production: Recent updates of pretreatment methods and the potential effect of humic and nutrients substances. *Proc. Saf. Environ.* **2021**, *145*, 321−339.
(46) Su, X.; Hu, J.; Zhang, J.; Liu, H.; Yan, C.; Xu, J.; Ma, Y.; Song, J. Investigating the adsorption behavior and mechanisms of insoluble Humic acid/starch composite microspheres for metal ions from water. *Colloids Surf., A* **2021**, *610*, 125672.
(47) Li, J.; Hao, X.; van Loosdrecht, M. C. M.; Liu, R. Relieving the inhibition of humic acid on anaerobic digestion of excess sludge by metal ions. *Water Res.* **2021**, *188*, 116541.
(48) Zhao, W.; Zhang, J.; Zhang, H.; Yang, M.; Zang, L. Comparison of mesophilic and thermophilic biohydrogen production amended by nickel−doped magnetic carbon. *J. Cleaner Prod.* **2020**, *270*, 122730.
(49) Zhang, J.; Zhao, W.; Zhang, H.; Wang, Z.; Fan, C.; Zang, L. Recent achievements in enhancing anaerobic digestion with carbon−based functional materials. *Bioresour. Technol.* **2018**, *266*, 555−567.
(50) Zhong, D.; Li, J.; Ma, W.; Xin, H. Magnetite nanoparticles enhanced glucose anaerobic fermentation for bio−hydrogen production using an expanded granular sludge bed (EGSB) reactor. *Int. J. Hydrogen Energy* **2020**, *45*, 10664−10672.
(51) Xu, R.; Yang, Z. H.; Zheng, Y.; Zhang, H. B.; Liu, J. B.; Xiong, W. P.; Zhang, Y. R.; Ahmad, K. Depth−resolved microbial community analyses in the anaerobic co−digester of dewatered sewage sludge with food waste. *Bioresour. Technol.* **2017**, *244*, 824−835.
(52) Yang, G.; Wang, J. Changes in microbial community structure during dark fermentative hydrogen production. *Int. J. Hydrogen Energy* **2019**, *44*, 25542−25550.
(53) Wang, C.; Liu, J.; Xu, X.; Zhu, L. Response of methanogenic granules enhanced by magnetite to ammonia stress. *Water Res.* **2022**, *212*, 118123.
(54) Fu, X.; Jin, X.; Pan, C.; Ye, R.; Wang, Q.; Wang, H.; Lu, W. Enhanced butyrate production by transition metal particles during the food waste fermentation. *Bioresour. Technol.* **2019**, *291*, 121848.
(55) Sim, Y. B.; Jung, J. H.; Baik, J. H.; Park, J. H.; Kumar, G.; Rajesh Banu, J.; Kim, S. H. Dynamic membrane bioreactor for high rate continuous biohydrogen production from algal biomass. *Bioresour. Technol.* **2021**, *340*, 125562.
(56) Mugnai, G.; Borruso, L.; Mimmo, T.; Cesco, S.; Luongo, V.; Frunzo, L.; Fabbricino, M.; Pirozzi, F.; Cappitelli, F.; Villa, F. Dynamics of bacterial communities and substrate conversion during olive−mill waste dark fermentation: Prediction of the metabolic routes for hydrogen production. *Bioresour. Technol.* **2021**, *319*, 124157.
(57) Feng, Q.; Song, Y. C.; Yoo, K.; Kuppanan, N.; Subudhi, S.; Lal, B. Influence of neutralization in acidic distillery wastewater on direct interspecies electron transfer for methane production in an upflow anaerobic bioelectrochemical reactor. *Int. J. Hydrogen Energy* **2017**, *42*, 27774−27783.
(58) Mo, H.; Wang, N.; Ma, Z.; Zhang, J.; Zhang, J.; Wang, L.; Dong, W.; Zang, L. Hydroxyapatite fabrication for enhancing biohydrogen production from glucose dark fermentation. *ACS Omega* **2022**, *7*, 10550−10558.
(59) Li, X.; Mo, H.; Zhou, C.; Ci, Y.; Wang, J.; Zang, L. Nickel foam promotes syntrophic metabolism of propionate and butyrate in anaerobic digestion. *ACS Omega* **2021**, *6*, 21033−21042.

https://doi.org/10.1021/acsomega.2c05580
ACS Omega 2022, 7, 41594−41605